

Pigment Transport in Paint Marbling

Aubrey G. Jaffer
agj@alum.mit.edu

Abstract

The swirling marbling patterns on the surface of a liquid bath can be mathematically modeled as area-preserving homeomorphisms. But motion while laying a piece of paper on the surface is not necessarily area-preserving, and can darken and lighten regions of the transferred image. In particular, elliptical motions in the plane of the surface can create forms looking like waves with broad crests and sharp troughs which, in combination with tinting and shading from those motions, produce a compelling three-dimensional visual effect.

The transfer mapping and shading transforms for periodic elliptical paper motions are presented and used to digitally render a “Spanish Wave” design similar to those produced by human marbling practitioners.

Certain combinations of solvent and pigment in paint can produce tinting and shading within each paint drop. A shading transform is presented for one class of such mixtures which is used by contemporary marblers.

Keywords

paint marbling; fluid mechanics; computer graphics

Table of Contents

<i>Introduction</i>	1
<i>Transfer Mapping</i>	2
<i>Inverse Transfer Mapping</i>	3
<i>Tinting</i>	5
<i>Spanish Wave</i>	6
<i>Pigment Transport Within Drops</i>	7
<i>Pivoting</i>	9
<i>Turkish Moire</i>	10
<i>Acknowledgments</i>	11

1. Introduction

Marbled designs are created by floating various color paints on a tank filled with “sizing” liquid, then moving a stylus or an array of styli (rake) through the bath.

Many paint marbling techniques can be mathematically described by closed-form homeomorphisms¹. An article analyzing marbling techniques is *Mathematical Marbling*[1]. The fluid mechanics of marbling are explored in *Oseen Flow in Paint Marbling*[2] and *The Lamb-Oseen Vortex and Paint Marbling*[3].

In order to preserve the design created in the tank, paper is laid onto the liquid’s surface; then peeled upward, capturing floating paint on its lower surface.

More than 150 years ago some marbling practitioners discovered that moving the paper while laying it on the bath had interesting effects on their captured designs. This article analyzes the effects of such motion.

Marbling practitioners have also discovered solvent-pigment combinations which produce nonuniform pigment profiles across single paint drops. A thickness profile proportional to the Gaussian probability distribution successfully models works by several marblers; it is analyzed in Section 6.

The transforms in this article and the three cited above are implemented in the `pst-marble`[4] L^AT_EX software package available from CTAN². The mathematical marbling images in this paper were generated using `pst-marble` version 1.6.

¹ A homeomorphism is a continuous function between topological spaces (in this case between a topological space and itself) that has a continuous inverse function.

² <https://ctan.org/pkg/pst-marble>

2. Transfer Mapping

Laying a paper starting from one end, the line of contact will move from the starting to opposite end. With sinusoidal paper movement, the vector function mapping liquid surface coordinates to paper is:

$$\left(\frac{A}{2} \sin \left[360 \frac{x \sin \theta + y \cos \theta + \Omega}{\lambda} \right], \frac{-B}{2} \cos \left[360 \frac{x \sin \theta + y \cos \theta + \Omega}{\lambda} \right], 1 \right) \begin{pmatrix} \sin \theta & \cos \theta \\ -\cos \theta & \sin \theta \\ x & y \end{pmatrix} \quad (1)$$

The A and B terms are the movement parallel and perpendicular (respectively) to the axis in the θ direction. Movement perpendicular to the θ axis is simply a sinusoidal function of distance along the θ axis. Consider movement along the θ axis as a function of $a = (x \sin \theta + y \cos \theta + \Omega)/\lambda$:

$$f(a) = a + \frac{A}{2} \sin \left(\frac{360 a}{\lambda} \right) \quad -\frac{1}{2} < \frac{a}{\lambda} < \frac{1}{2} \quad (2)$$

For the inverse of $f(a)$ to be a function, $f(a)$ must be strictly monotonic and:

$$0 < f'(a) = 1 + \frac{\pi A}{\lambda} \cos \left(\frac{360 a}{\lambda} \right) \quad \left| \frac{\pi A}{\lambda} \right| < 1 \quad (3)$$

So the line of contact moves from one end of the sheet to the other, without pausing or backtracking.



Figure 1

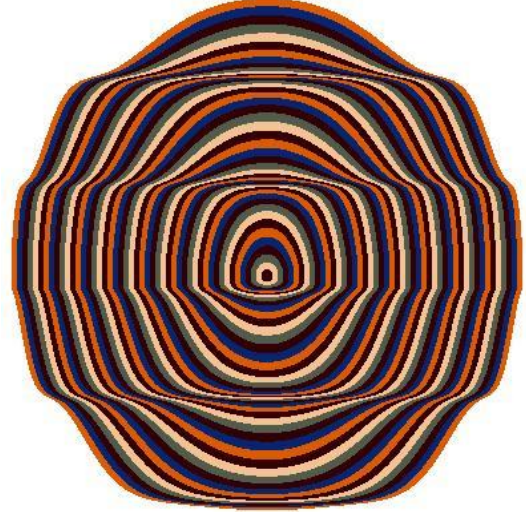


Figure 2



Figure 3



Figure 4

Figures 1 through 4 all have $\lambda = 200$. Figure 1 has $A = 0$, $B = 45$, and is area-preserving. Figure 2 has $A = 45$ and $B = 0$; bands of vertical expansion and compression alternate. Figure 3 is the combination of Figure 1 and Figure 2 with $A = 45$ and $B = 45$; but the compression bands have become creases! The horizontal wiggle and $f'(a)$ both reach their maximums at $a \equiv 0 \pmod{\lambda}$, which vertically compresses the neighborhood around $a \equiv 0 \pmod{\lambda}$.

Figure 4 is the same design as Figure 3, but rendered from the paper's coordinate system using the formulas of Section 3.

3. Inverse Transfer Mapping

Raster rendering starts with a pixel position on the paper and computes the tank coordinates it came from. So $f^{-1}(a)$ is needed for raster rendering. The family of curves in the positive-positive quadrant of Figure 5 resembles $g(a) = 0.5 \lambda (2a/\lambda)^\chi$ where $0 < \chi$ and $0 < 2a/\lambda < 1$.

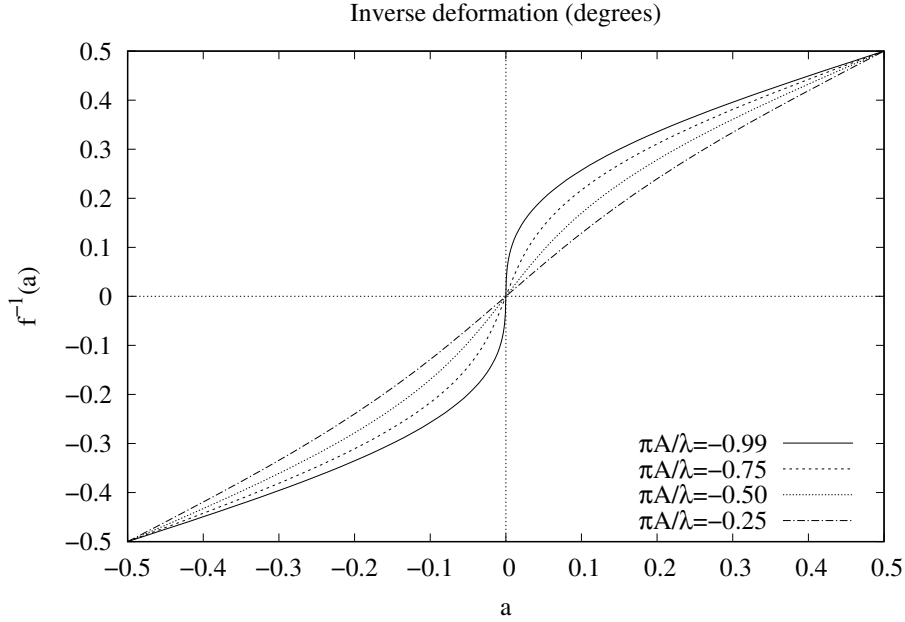


Figure 5

Functions $g(a)$ and $f^{-1}(a)$ match at $a = 0$ and $a = \lambda/2$. The slope of $f^{-1}(0)$ is singular. Matching the slopes at $a = \lambda/2$:

$$\begin{aligned}
 g(a) &= \frac{\lambda}{2} \left(\frac{2a}{\lambda} \right)^\chi & g'(a) &= \frac{\chi\lambda}{2a} \left(\frac{2a}{\lambda} \right)^\chi \\
 g'(\lambda/2) &= \chi & f'(\lambda/2) &= 1 - \frac{2\pi A}{\lambda} \\
 g'(\lambda/2) &= 1/f'(\lambda/2) & \chi &= \frac{1}{1 - \pi A/\lambda}
 \end{aligned} \tag{4}$$

Figure 6 compares $f^{-1}(a)$ with $g(a)$ where $\chi = (4/3)/[1 - \pi A/\lambda]$, which is a better match than equation (4).

While the slopes at the upper ends of the curves match well, the slopes near $a = 0$ are more important visually. The moderate slopes of $g(a)$ do not produce the crisp bends achieved by marbling practitioners. However, $g(a)$ is close to f^{-1} and makes a good initial value for the Newton-Raphson method:

$$g_1(a) = g(a) - \frac{f(g(a)) - a}{f'(g(a))} = g(a) - \frac{g(a) + (A/2) \sin(360g(a)/\lambda) - a}{1 + (\pi A/\lambda) \cos(360g(a)/\lambda)} \tag{5}$$

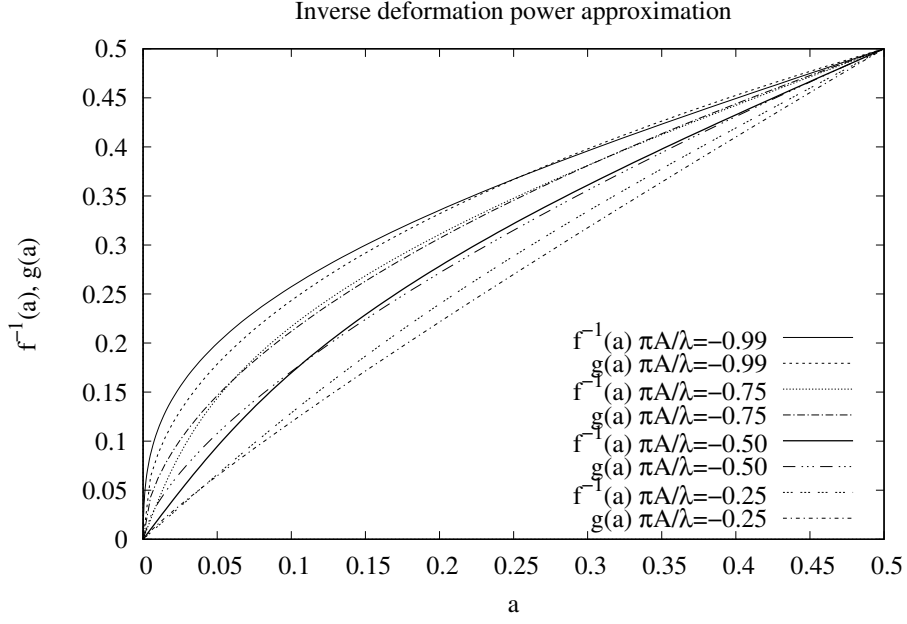


Figure 6

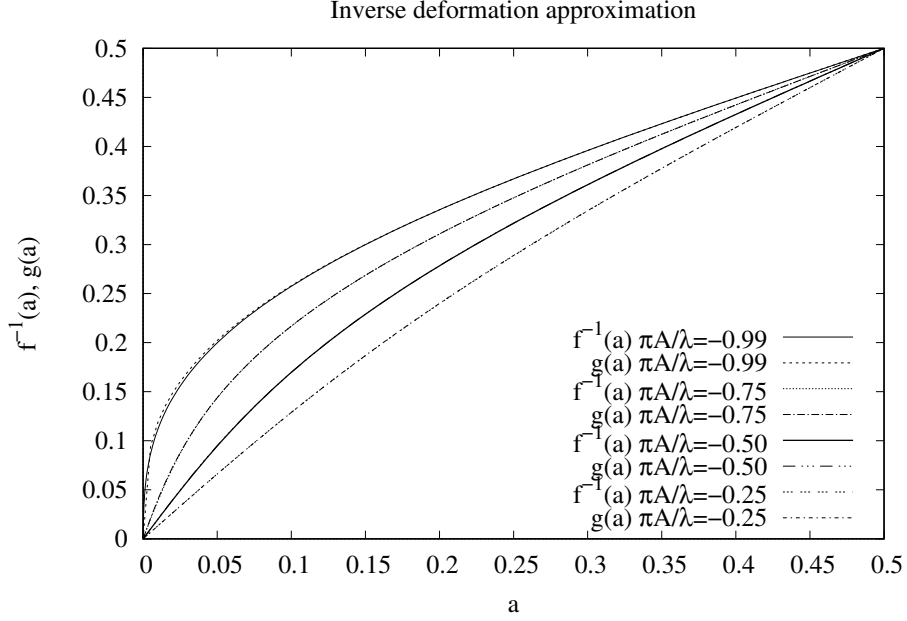


Figure 7

Figure 7 shows that one iteration of the Newton-Raphson method is sufficient. Extending $g(a)$ to all combinations of signs:

$$g(a) = \left| \frac{\lambda}{2} \right| \text{sign}(a) \begin{cases} |2a/\lambda|^{(4/3)/(1+|\pi A/\lambda|)}, & \text{if } \frac{A}{\lambda} < 0; \\ 1 - [1 - |2a/\lambda|]^{(4/3)/(1+|\pi A/\lambda|)}, & \text{if } \frac{A}{\lambda} > 0. \end{cases} \quad (6)$$

In equation (1), the perpendicular displacement is a function of a ; the same is true for the derivative of $f(a)$ from equation (3). In raster rendering the perpendicular term and f' are computed from $g_1(a)$ instead of a .

4. Tinting

While the paper is pushed in the opposite direction from the line of contact progress, the layer of paint adhering to the paper's line of contact will be thinner than when the paper is being simply layed. So the pigment concentration on the paper varies inversely with the derivative of $f(a)$ from equation (3). The maximum value of $f'(a)$ is 2; so the concentration can only decrease to half of nominal. If the paint is opaque at half of nominal thickness, then color will not be affected by transfer to paper and the rest of this section doesn't apply.

The popular RGB system for specifying colors is an additive color system; but pigments on paper are a subtractive color process. In rendering an image, the pigment thickness is not perceivable, but the optical density is. Normalizing the 0 to 255 color component range to values between 0 and 1, this RGB formula behaves correctly in the corner-cases and produces plausible colors:

$$[1 - (1 - I_r)^\gamma, 1 - (1 - I_g)^\gamma, 1 - (1 - I_b)^\gamma] \quad \gamma = f'(a) \quad (7)$$

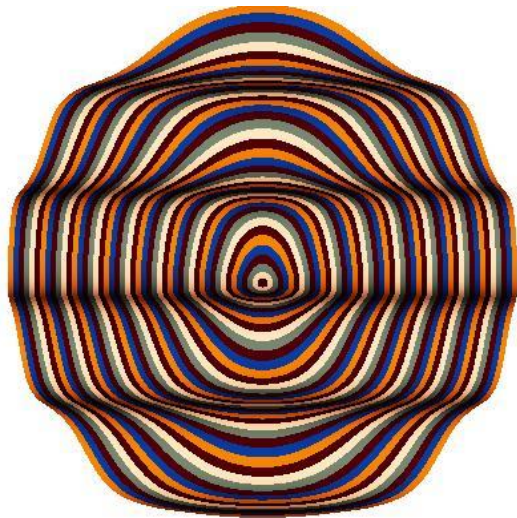


Figure 8



Figure 9



Figure 10



Figure 11

Figures 8 and 9 render Figures 2 and 3 with shading where $A = 45$ is the same value as the deformation. In Figure 10, shading $A = 35$ in the left half and $A = 63$ in the right half (with deformation $A = 45$). With $\lambda = 200$ the largest possible $A = \lambda/\pi \approx 63.6$; Figure 11 shows deformation and shading $A = 63$.

5. Spanish Wave

Figure 12 shows a photograph of a “Spanish Wave” pattern from the end-paper of a book bound in France circa 1843³. Figure 13 shows a mathematically produced pattern. Large teal drops were placed randomly into a scrambled pattern of yellow in a mauve background. A spray of slightly lighter teal (but still shaded) was applied to add texture. Two sinusoidal deformations at slightly different orientations were superimposed to recreate the variation in wavelengths.

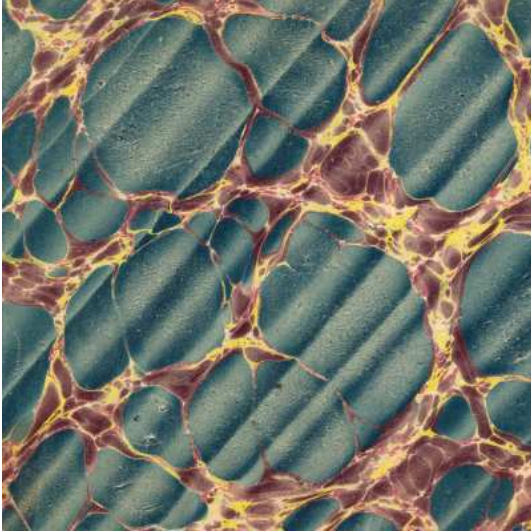


Figure 12

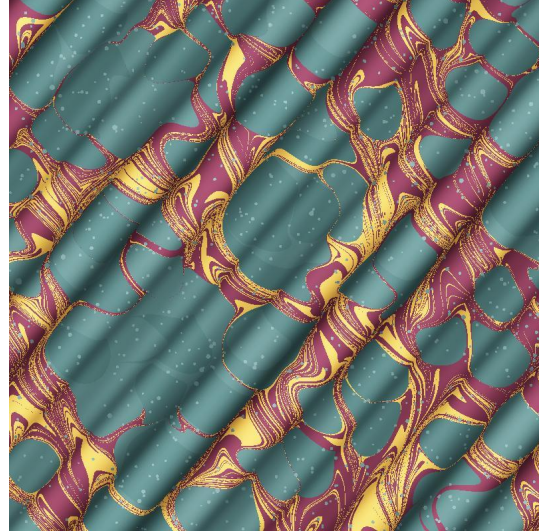


Figure 13



Figure 14



Figure 15

Figure 14 converts a nonpareil pattern into seeming cylinders.

Creasing the paper before placing it on the liquid’s surface creates an effect similar to the Spanish wave, but can intersect waves at different angles. Figure 15 shows a mathematical marbling with waves intersecting at right angles.

³ Creator of the paper marbling unknown, but dead for more than 70 years; image scanned and slightly edited by Aristeas. [Public domain], from Wikimedia Commons

6. Pigment Transport Within Drops

Certain combinations of solvent and pigment do not produce a uniformly colored disk when dropped onto the sizing in the tank; the solvent pushes out further than it carries the pigment, leaving the center of the disk darker than its edges. For the disk of paint from a vertical drop the pigment thickness will be radially symmetric and be proportional to a normal distribution which peaks at the disk's center:

$$\exp\left(\frac{-\zeta a^2}{r^2}\right) \quad (8)$$

where a is the point's distance from the disk center, r is the disk's radius, and ζ is a shape factor. When $\zeta = 0$ the paint disk is uniform. The normalized thickness is found by dividing formula (8) by the thickness averaged over the disk:

$$\exp\left(\frac{-\zeta a^2}{r^2}\right) \Big/ \int_0^r \exp\left(\frac{-\zeta a^2}{r^2}\right) \frac{da}{\pi r^2} = \exp\left(\frac{-\zeta a^2}{r^2}\right) \left(\frac{\zeta \exp(\zeta)}{\exp(\zeta) - 1}\right)$$

As in color formula (7), γ is the reciprocal of the normalized pigment thickness:

$$[1 - (1 - I_r)^\gamma, 1 - (1 - I_g)^\gamma, 1 - (1 - I_b)^\gamma] \quad \gamma = \exp\left(\frac{\zeta a^2}{r^2}\right) \left(\frac{\exp(\zeta) - 1}{\zeta \exp(\zeta)}\right)$$

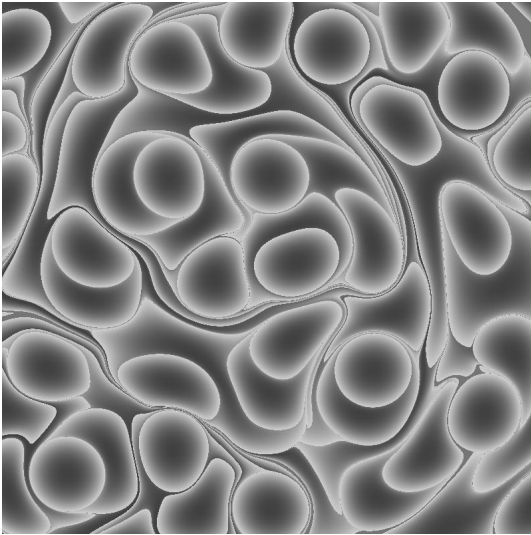


Figure 16

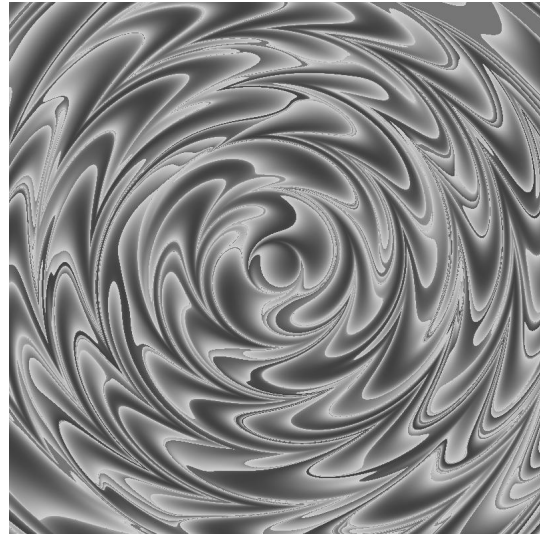


Figure 17

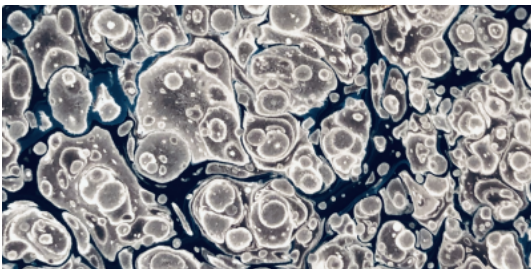


Figure 18

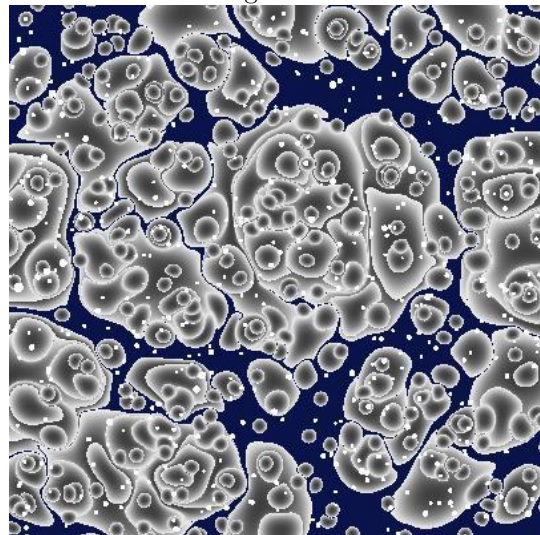


Figure 19

Figure 16 shows the computed pattern resulting from 25 randomly placed drops of radius 0.1 followed by 50 drops of radius 0.071, all with the same pigment color and $\zeta = 1.75$. Figure 17 shows the same process followed by a rake with 0.1 tine spacing being spun counterclockwise.

Figure 18 from Dan and Regina St.John⁴ shows their “shell” pattern resulting from walnut-oil being added to the paint. The mathematical marbling in Figure 19 required $\zeta = 2.25$ to match the contrast. The small drops are round in Figure 19, unlike in Figure 18 where tapping a paintbrush produced horizontal spray.

Figure 20 shows a Spanish wave marbling created by Galen Berry⁵ which also has drop-shading. It achieves a three-dimensional appearance with $B = 0$; the paper was not moved laterally. Figure 21 shows a similar mathematical marbling with $\lambda = 0.12$ and $A = 0.015$; the ringed drops have $\zeta = 0.5$ (smaller, lighter drops have $\zeta = 0.2$).

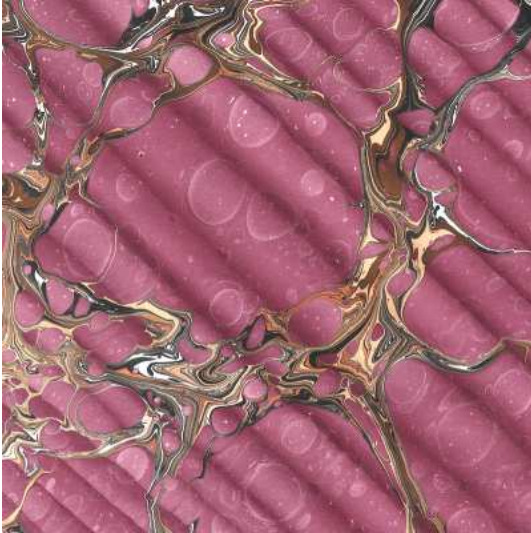


Figure 20

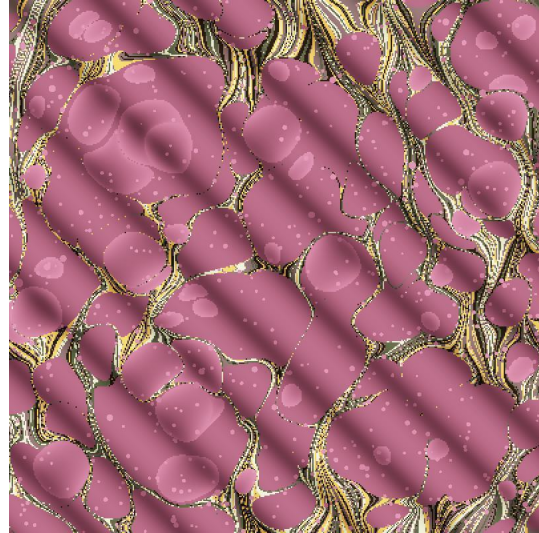


Figure 21

⁴ Used with permission.

⁵ Used with permission.

7. Pivoting

Rather than laterally shifting the paper while laying it in the tank, one could pivot the paper around one corner. Figure 22 shows the result of just pivoting around the lower left corner while laying down the paper. Figure 23 shows the result of radial motion without pivoting. Figure 24 shows the combination, which looks very similar to Figure 25, the result of rotating a rake counterclockwise around the lower left corner.

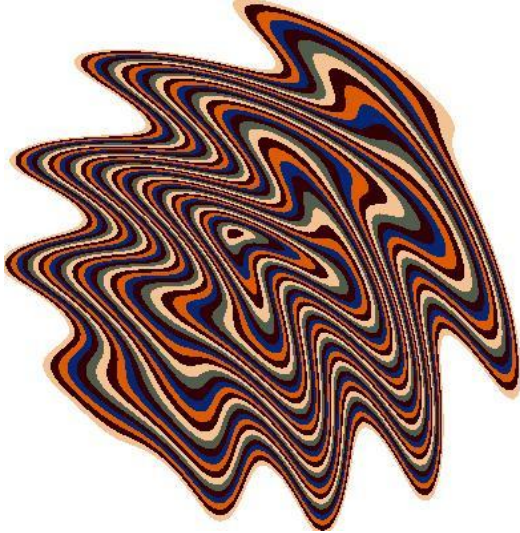


Figure 22



Figure 23

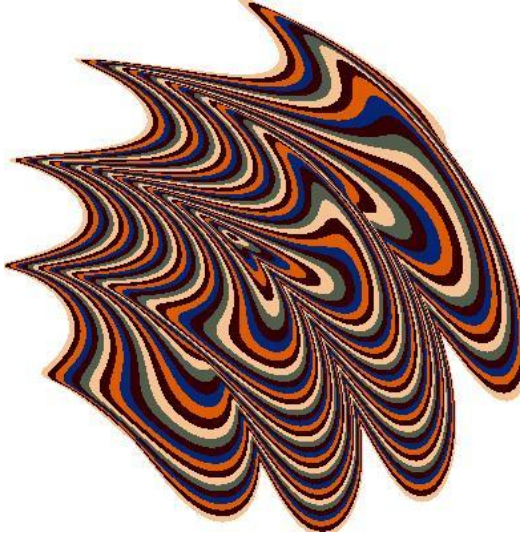


Figure 24

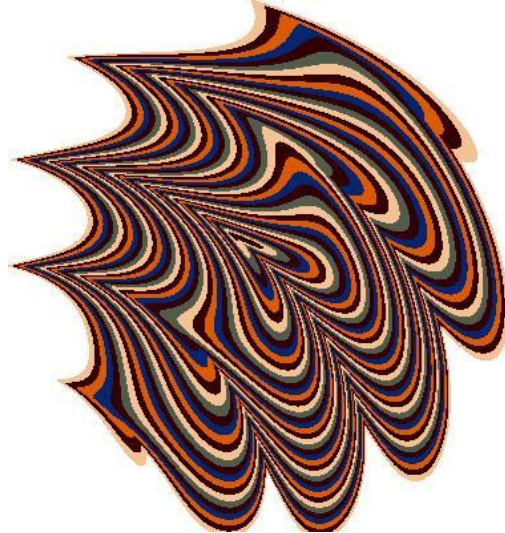


Figure 25

8. Turkish Moire

Most Turkish moire marblings are like Spanish wave, but with curved shading contours. Dan and Regina St.John sent me photographs of some Turkish moire patterns which, in addition to having sharply curved shading contours, had shading which was reversed from the usual. Instead of the areas of stretched paint having lighter tone, they were darker than the areas of compressed paint.

The subtractive model of formula (7) works only if the paper tone is lighter than the paint tone. The paint must act in an additive fashion in order to be visible on a black background.

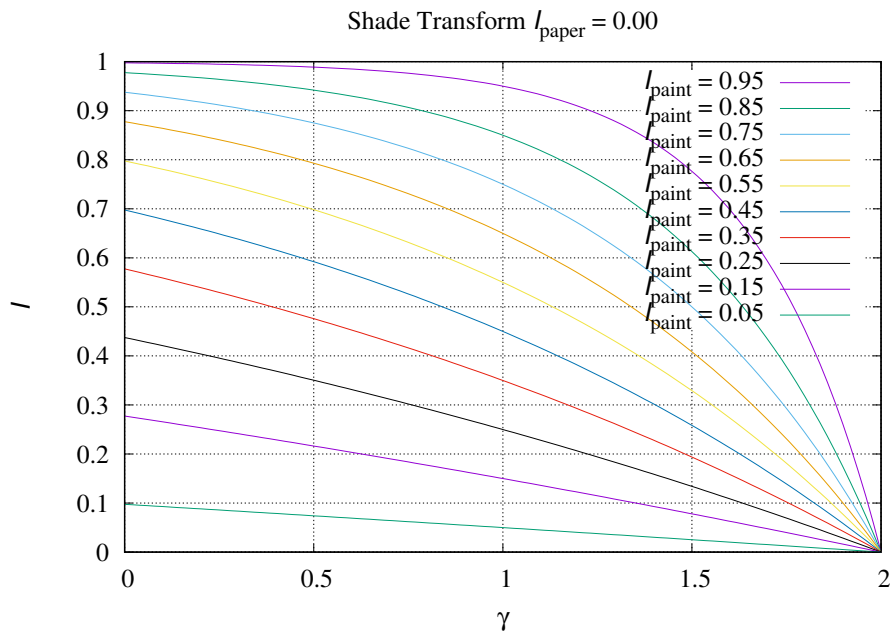
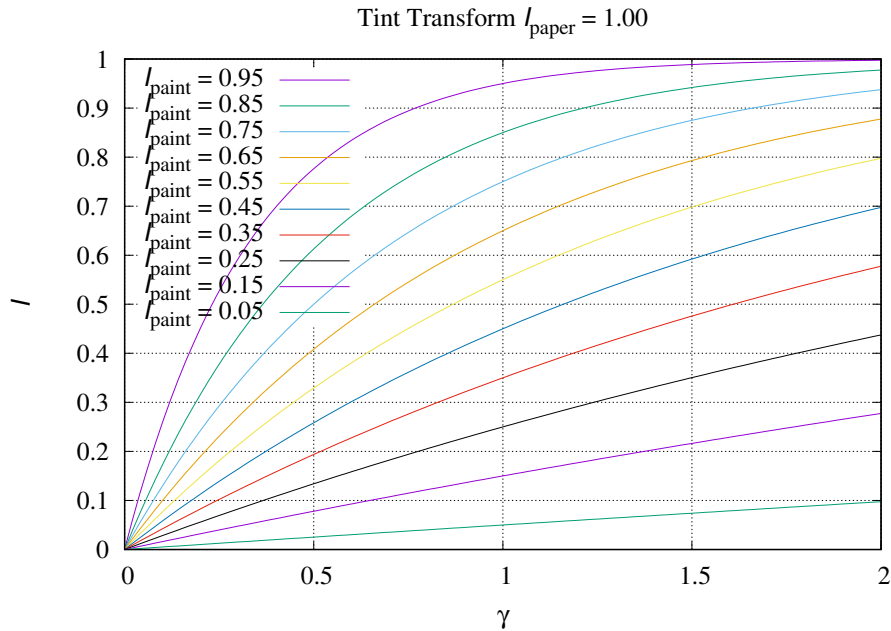


Figure 26 shows the intensity transfer function for equation (9) for white paper, $I_{paper} = 1$. Figure 27 shows the intensity transfer function for black paper, $I_{paper} = 0$. Figure 28 shows the intensity transfer function for gray paper, $I_{paper} = 0.5$. Unfortunately there is a discontinuity between paper darker than

paint and paint darker than paper with $\gamma < 1$; formula (9) needs further development.

$$I = \begin{cases} I_{paper} \left[1 - \left(1 - \frac{I_{paint}}{I_{paper}} \right)^\gamma \right], & \text{if } I_{paper} \geq I_{paint}; \\ 1 - (1 - I_{paper}) \left(\frac{1 - I_{paint}}{1 - I_{paper}} \right)^{2-\gamma}, & \text{if } I_{paper} < I_{paint}. \end{cases} \quad (9)$$

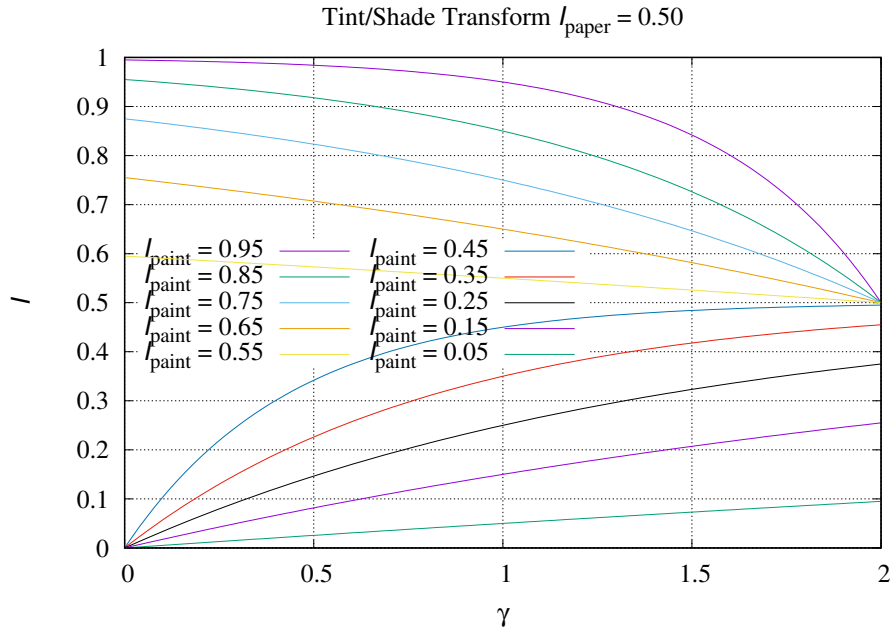


Figure 28

Figure 29 shows a Turkish moire-like marbling with curved shading contours on black paper.

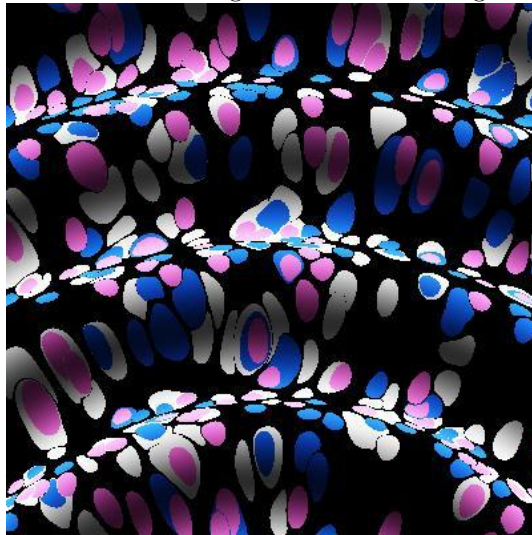


Figure 29

9. Acknowledgments

Thanks to Dan and Regina St.John of Chena River Marblers and Galen Berry at MarbleArt.US for sharing their marbling knowledge and examples of their works.

References

- [1] Shufang Lu, A. Jaffer, Xiaogang Jin, Hanli Zhao, and Xiaoyang Mao. Mathematical marbling. *IEEE Computer Graphics and Applications*, 32(6):26–35, 2012.
- [2] A. Jaffer. Oseen Flow in Ink Marbling. *ArXiv e-prints*, January 2017.
- [3] A. Jaffer. The Lamb-Oseen Vortex and Paint Marbling. *ArXiv e-prints*, October 2018.
- [4] Aubrey Jaffer, Jürgen Gilg, and Manuel Luque. `pst-marble`, 2019. version 1.6.